Cite as: Z. Xiang *et al.*, *Science* 10.1126/science.aap9607 (2018).

Quantum oscillations of electrical resistivity in an insulator

Z. Xiang[1], Y. Kasahara[2], T. Asaba[1], B. Lawson[1,3], C. Tinsman[1], Lu Chen[1], K. Sugimoto[4], S. Kawaguchi[4], Y. Sato[2], G. Li[1], S. Yao[5], Y. L. Chen[6], F. Iga[7], John Singleton[8], Y. Matsuda[2]*, Lu Li[1]*

[1]Department of Physics, University of Michigan, Ann Arbor, MI 48109, USA. [2]Department of Physics, Kyoto University, Kyoto 606-8502, Japan. [3]Faculty of Applied Science, Université Chrétienne Bilingue du Congo, Beni, North-Kivu, Democratic Republic of Congo. [4]Japan Synchrotron Radiation Research Institute, Sayo, Hyogo 679-5198, Japan. [5]National Laboratory of Solid State Microstructures, Nanjing University, Nanjing 210093, China. [6]Department of Physics, Clarendon Laboratory, University of Oxford, Oxford, OX1 3PU, UK. [7]College of Science, Ibaraki University, Mito 310-8512, Japan. [8]National High Magnetic Field Laboratory, Los Alamos National Laboratory, Los Alamos, NM 87545, USA.

***Corresponding author. Email: luli@umich.edu (L.L.); matsuda@scphys.kyoto-u.ac.jp (Y. M.)**

In metals, orbital motions of conduction electrons on the Fermi surface are quantized in magnetic fields, which is manifested by quantum oscillations in electrical resistivity. This Landau quantization is generally absent in insulators. Here we report a notable exception in an insulator — ytterbium dodecaboride (YbB_{12}). The resistivity of YbB_{12}, which is of a much larger magnitude than the resistivity in metals, exhibits distinct quantum oscillations. These unconventional oscillations arise from the insulating bulk, even though the temperature dependence of the oscillation amplitude follows the conventional Fermi liquid theory of metals with a large effective mass. Quantum oscillations in the magnetic torque are also observed, albeit with a lighter effective mass.

In Kondo insulators, the hybridization between itinerant and localized electrons opens an insulating gap, and consequently their resistivity diverges at low-temperature (*1*, *2*). Recently there has been a lively debate about the nature of the ground state of Kondo insulator samarium hexaboride (SmB_6) in intense magnetic fields. Although mixed-valence SmB_6 is a good insulator (its resistance increasing by five orders of magnitude when cooled down to 300 mK from room temperature), Landau level (LL) quantization still occurs and clear quantum oscillations are observed in its magnetization (the de Haas-van Alphen, or dHvA, effect) (*3*, *4*). The origin and interpretation of the dHvA oscillations in SmB_6 have been highly controversial, owing to a number of peculiar features. First, the oscillations are observed only in magnetization, and not in electrical resistivity (the Shubnikov-de Haas, or SdH, effect). Second, unlike the heavy carriers revealed by the thermoelectric studies (*5*), oscillations appear to arise from quasiparticles with a very light effective mass ($m = m_e$, m_e is the free electron mass) (*3*). Third, in floating-zone grown SmB_6 samples, the dHvA signal exhibits a striking deviation from the standard Lifshitz-Kosevich (LK) formula in Fermi-liquid theory (*4*). These observations point to either a topologically protected surface state (*3*), or the presence of an unconventional Fermi surface in an insulator (*4*). A number of intriguing physical origins have been proposed, including exciton-based magnetic breakdown (*6*, *7*), Majorana type charge-neutral Fermi surfaces (*8*), a failed superconducting ground state (*9*), and spinon Fermi surfaces (*10*, *11*). A key to solving the most fundamental problem, the existence of "a Fermi surface in an insulator", lies in clarifying if quantum oscillations, in particular in charge transport, are observable in another insulating system.

Here we present quantum oscillation studies of YbB_{12}, another cubic-structured rare-earth intermetallic compound. YbB_{12} has long been known as a mixed valence Kondo insulator (*12*–*14*). It behaves as a monovalent metal with localized magnetic moments at room temperature, whereas a nonmagnetic insulating ground state develops at low temperatures. The opening of a narrow energy gap of 10-15 meV at the Fermi level has been confirmed by many experiments (*15*–*17*) and is attributed to the hybridization between the itinerant 5*d* and the localized 4*f* electrons. The mean valence of Yb ions in YbB_{12} is +2.9 (*18*), close to $4f^{13}$ (+3) configuration. Therefore, the *f*-electrons are mostly localized and the crystalline electric field (CEF) ground state is well defined. In contrast, as the mean valence of Sm ions in SmB_6 is +2.6 (*19*), *f*-electrons are more itinerant and the CEF scheme is not well defined. Therefore, the electronic structure of YbB_{12} is much simpler than that of SmB_6. Furthermore, early calculations in YbB_{12} predicted the existence of topological surface states owing to mirror-symmetry protection (*20*).

YbB_{12} single crystals are grown in a floating-zone furnace [Section 1 of (*21*)]. Using the experimental setup shown in Fig. 1A, magnetic torque and magnetoresistance (MR) are measured up to 45 T simultaneously [Section 2 of (*21*)]. The temperature dependence of the resistivity (Fig. 1B) confirms an

increase of five orders of magnitude from room temperature to 50 mK. The resistivity has a weak temperature dependence below 2.2 K, resembling the resistive "plateau" well known in SmB_6 at $T < 3.5$ K (*22*). This "plateau" is an indication of the existence of extended in-gap states. Fitting with the thermal activation model of resistivity, $\rho(T) = \rho_0 \exp(\Delta/2k_BT)$, reveals a two-gap feature with the gap width 12.5 meV (20 K < T < 40 K) and 4.7 meV (6 K < T < 12.5 K), respectively (Fig. 1B, inset), consistent with previous transport results (*23*). Upon applying the magnetic field, the negative slope of the $\rho(T)$ curve is preserved up to 45 T with no hints of metallic behavior (Fig. 1C), indicating that the ground state is still gapped (see fig. S5 for more information).

The field dependence of the magnetic torque in the insulating state of YbB_{12} is shown in Fig. 1D. We observe a step-increase at 20 T followed by a decrease at 28 T. These features are weak metamagnetic transitions and/or crossovers that could potentially be related to the predicted field-induced staggered magnetism in Kondo insulators (*24*). Above approximately 37.5 T, the dHvA oscillations are clearly resolved (Fig. 1D). We note that the dHvA oscillations appear well below the insulator-metal (I-M) transition field in our YbB_{12} samples, which is determined to be 45.3 T-47.0 T by pulsed field studies [see Sections 4 and 5 of (*21*)]. Fast Fourier Transform (FFT) on the $\phi = 11.3°$ torque curve gives a dHvA frequency of F = 720 T (Fig. 1D, inset).

In Fig. 2A the MR data at $\phi = 27.7°$ is plotted between 11.5 T and 45 T. Given the zero-field resistivity $\rho(0) = 4.67\ \Omega$ cm of this sample at 350 mK, a significant negative MR ($\{\rho(H) - \rho(0)\}/\rho(0)$) of –95.9% is achieved at 45 T (a detailed angular dependence of MR is shown in fig. S3). The negative MR is a hallmark of Kondo insulators that results from field suppression of the hybridization gap (*25–28*). We note that the negative MR in YbB_{12} is much larger than that in SmB_6 (*29*, *30*). This is probably a consequence of the larger effective Landé g-factor in YbB_{12}, which increases the influence of the magnetic field (*17*, *28*). As H increases, MR displays wiggle-like features at around 16 T and 28 T. These wiggles do not arise from quantum oscillations because their positions are obviously temperature dependent (fig. S7); instead they are likely to be field-induced transitions/crossovers. The feature at 28 T is probably linked to the kink feature in the magnetic torque [Section 6 of (*21*)].

The most striking result in Fig. 2A are the oscillations that appear in the MR under strong magnetic fields. From 40.8 T up to 45 T, two valleys and one peak in total can be clearly observed (Fig. 2A, upper inset). The FFT on the MR oscillations in this field regime yields a clear frequency peak at F = 913 T Fig. 2A, lower inset). With the magnetic field direction close to the crystal axes, up to four oscillation periods can be seen (Fig. 2B). The overall SdH patterns are almost identical for $\phi = 11.3°$ and $\phi = 78.4°$, whereas there is a small valley position shift between $\phi = 18.3°$ and $\phi = 70.5°$. This suggests an axis of symmetry along [101] direction for the SdH oscillations, which is consistent with the cubic structure of YbB_{12} crystal (fig. S10). The fact that the valleys in $d\rho/dH$ in Fig. 2B are approximatly uniformly spaced as a function of $1/H$ provides strong evidence that the SdH oscillations have a single dominating frequency. These overall patterns of the SdH oscillations, as well as those of the dHvA oscillations, are well reproduced between different YbB_{12} samples [Section 3 of (*21*)].

The observation of the SdH oscillations is reinforced by the T-dependence of oscillation amplitudes. The evolution of the high-field wiggle features in both MR and torque data show the typical behavior of quantum oscillations, with T-independent positions of the dominant peaks/valleys within the uncertainty, and an attenuated amplitude from base temperature up to 1.5 K (figs. S7 and S8). The T-dependent amplitudes of normalized oscillatory torque (Fig. 3A) and oscillatory MR (Fig. 3, B and C) are fitted using the conventional LK formula (*31*). The fittings are reasonably good down to 60 mK, indicating that the LK expression, based on the Fermi liquid framework, appears to be valid in the Kondo insulator YbB_{12}. The agreement with the LK description confirms that the features we resolve are quantum oscillations rather than successive field-induced Lifshitz transitions.

The SdH oscillations are much more suppressed at higher T compared to dHvA oscillations at the same angle (Fig. 3, A and B), revealing a heavier effective mass in the electrical transport channel. The effective masses of the quasiparticles estimated from the dHvA and SdH oscillations at the same tilt angle are approximately 6.6 m_e and 14.6 m_e, respectively. Therefore it is unlikely that both types of oscillations originate from the same band. Indeed the SdH and dHvA frequencies have different angle dependences (Fig. 4). The dHvA frequencies F can be tracked by a two-dimensional (2D) Fermi surface model ($F \propto \frac{1}{\cos\theta}$) with the in-plane cross section area $A_{[001]}$ = 6.67 nm^{-2} (solid line in Fig. 4). Given the lack of dHvA oscillations observed above $\simeq 20°$ (figs. S3 and S9), this inverse sinusoidal dependence can be explained by either a 2D Fermi cylinder, or a heavily elongated 3D Fermi pocket. On the other hand, the angular dependence of the SdH frequencies displays a clearly nonmonotonic behavior: a frequency maximum appears at Θ ~ 15-20° from the crystal axes, resulting in an "M"-shape with a local dip at $H \parallel$ [100] and a fast decrease in the frequency beyond the maximum. The 2D Fermi surface model apparently can not describe this behavior. Our attempt to model the SdH frequencies (Fig. 4, dashed lines, and figs. S1 and S10) points to hyperbolic "neck" orbits [Section 8 of (*21*)].

The amplitude of the quantum oscillations is determined by a combination of temperature, band curvature, Dingle and spin factors. Assuming Dingle and spin factors do not depend on the band, the oscillation amplitude of the light band with the 2D character should be much larger than that of the heavy band with the 3D character. As the observed SdH oscillations arise from a relatively heavy band ($m^* \approx 15\ m_e$), it is highly unusual that the oscillations observed in the dHvA effect, which detects the orbits from a much lighter band ($m^* \approx 6.6\ m_e$), are not present in the SdH effect. The Section 11 of (*21*) will discuss the possible origins of the dHvA oscillations, based on either surface state (*32*), or charge-neutral Fermi surface (*10*), or a minority phase. Further, based on the symmetry analysis and other tests in a even stronger magnetic field, we note that the bulk SdH oscillations do not arise from metallic impurity phases [Section 7, 9 and 10 of (*21*)], or from a minority portion of sample which has a lower I-M transition field [Section 4 and 5 of (*21*)].

There are several notable features in the SdH oscillations we observed. The effective masses obtained from LK fittings are large, in agreement with the nature of a Kondo insulator in which strong electron correlations make the quasiparticles heavy. Even in the insulating state, a finite electronic specific heat coefficient γ is observed in YbB_{12} (*33*). Interestingly, assuming a spherical Fermi surface with $k_F \sim 0.156$ Å^{-1} ($F = 800$ T) and effective mass $m^* = 15\ m_e$ obtained from the SdH oscillations, the value of γ is calculated to be 7.6 mJ/mol K^2, comparable to the observed value of $\gamma \sim 8$ mJ/mol K^2 at 39 T (*33*). The background resistivity ρ still has a magnitude of more than 100 mΩ cm above 40 T, which is well beyond that of normal metals (*34*). Indeed if we estimate the mean free path ℓ by considering a spherical Fermi surface with $m^* = 15\ m_e$ and setting $\rho = 0.4\ \Omega$ cm (Fig. 2A), we will obtain an unphysically short mean free path, $\ell \sim 0.01$ nm.

Unconventional quantum oscillations have been proposed in insulators with hybridization gaps (*6*–*11*, *35*, *36*). However, our discovery of quantum oscillations in charge transport can not be effectively interpreted by the theories that either invoke charge-neutral quasiparticles (*7*–*9*) or associate the oscillations with the grand canonical potential (*6*). More importantly, all these theories of exotic quantum oscillations predict that in a gapped system the temperature dependence of the oscillation amplitude deviates from the conventional LK-formula at certain elevated temperatures. In contrast, our observations show that in YbB_{12} the LK formula works from $T = 1.5$ K (0.13 meV) down to $T = 60$ mK (0.0052 meV), i.e, a range of energy lower than both the hybridization gap width and the cyclotron energy of charge carriers at a field of $\simeq 40$ T [Section 11 of (*21*)]. Recent theories suggest an emergent neutral Fermi sea can exist in a mixed-valence gapped system and exhibit both dHvA and SdH oscillations (*10*, *11*), which may shed light on the exotic SdH oscillations we resolved, although a deviation from LK formula is still required in this scenario. A proper theory is yet to be established to describe the quantum oscillations observed in YbB_{12} under high magnetic field.

REFERENCES AND NOTES

1. H. Tsunetsugu, M. Sigrist, K. Ueda, The ground-state phase diagram of the one-dimensional Kondo lattice model. *Rev. Mod. Phys.* **69**, 809–864 (1997). doi:10.1103/RevModPhys.69.809
2. P. S. Riseborough, Heavy fermion semiconductors. *Adv. Phys.* **49**, 257–320 (2000). doi:10.1080/000187300243345
3. G. Li, Z. Xiang, F. Yu, T. Asaba, B. Lawson, P. Cai, C. Tinsman, A. Berkley, S. Wolgast, Y. S. Eo, D.-J. Kim, C. Kurdak, J. W. Allen, K. Sun, X. H. Chen, Y. Y. Wang, Z. Fisk, L. Li, Two-dimensional Fermi surfaces in Kondo insulator SmB_6. *Science* **346**, 1208–1212 (2014). doi:10.1126/science.1250366 Medline
4. B. S. Tan, Y.-T. Hsu, B. Zeng, M. C. Hatnean, N. Harrison, Z. Zhu, M. Hartstein, M. Kiourlappou, A. Srivastava, M. D. Johannes, T. P. Murphy, J.-H. Park, L. Balicas, G. G. Lonzarich, G. Balakrishnan, S. E. Sebastian, Heavy fermions. Unconventional Fermi surface in an insulating state. *Science* **349**, 287–290 (2015). doi:10.1126/science.aaa7974 Medline
5. Y. Luo, H. Chen, J. Dai, Z. Xu, J. D. Thompson, Heavy surface state in a possible topological Kondo insulator: Magnetothermoelectric transport on the (011) plane of SmB 6. *Phys. Rev. B* **91**, 075130 (2015). doi:10.1103/PhysRevB.91.075130
6. J. Knolle, N. R. Cooper, Quantum Oscillations without a Fermi Surface and the Anomalous de Haas-van Alphen Effect. *Phys. Rev. Lett.* **115**, 146401 (2015). doi:10.1103/PhysRevLett.115.146401 Medline
7. J. Knolle, N. R. Cooper, Excitons in topological Kondo insulators: Theory of thermodynamic and transport anomalies in SmB_6. *Phys. Rev. Lett.* **118**, 096604 (2017). doi:10.1103/PhysRevLett.118.096604 Medline
8. G. Baskaran, Preprint at http://arxiv.org/abs/1507.03477 (2015).
9. O. Erten, P.-Y. Chang, P. Coleman, A. M. Tsvelik, Skyrme Insulators: Insulators at the Brink of Superconductivity. *Phys. Rev. Lett.* **119**, 057603 (2017). doi:10.1103/PhysRevLett.119.057603 Medline
10. D. Chowdhury, I. Sodemann, T. Senthil, Mixed-valence insulators with neutral Fermi surfaces. *Nat. Commun.* **9**, 1766 (2018). doi:10.1038/s41467-018-04163-2 Medline
11. I. Sodemann, D. Chowdhury, T. Senthil, Quantum oscillations in insulators with neutral Fermi surfaces. *Phys. Rev. B* **97**, 045152 (2018). doi:10.1103/PhysRevB.97.045152
12. M. Kasaya, F. Iga, K. Negishi, S. Nakai, T. Kasuya, A new and typical valence fluctuating system, YbB12. *J. Magn. Magn. Mater.* **31-34**, 437–438 (1983). doi:10.1016/0304-8853(83)90312-8
13. M. Kasaya, F. Iga, M. Takigawa, T. Kasuya, Mixed valence properties of YbB12. *J. Magn. Magn. Mater.* **47-48**, 429–435 (1985). doi:10.1016/0304-8853(85)90458-5
14. T. Kasuya, Gap State in YbB_{12} and SmB_6 : Real Kondo Insulators. *Europhys. Lett.* **26**, 277–281 (1994). doi:10.1209/0295-5075/26/4/007
15. J.-M. Mignot, P. A. Alekseev, K. S. Nemkovski, L.-P. Regnault, F. Iga, T. Takabatake, Evidence for Short-Range Antiferromagnetic Fluctuations in Kondo-Insulating YbB 12. *Phys. Rev. Lett.* **94**, 247204 (2005). doi:10.1103/PhysRevLett.94.247204
16. M. Okawa, Y. Ishida, M. Takahashi, T. Shimada, F. Iga, T. Takabatake, T. Saitoh, S. Shin, Hybridization gap formation in the Kondo insulator YbB 12 observed using time-resolved photoemission spectroscopy. *Phys. Rev. B* **92**, 161108 (2015). doi:10.1103/PhysRevB.92.161108
17. T. T. Terashima, A. Ikeda, Y. H. Matsuda, A. Kondo, K. Kindo, F. Iga, Magnetization Process of the Kondo Insulator YbB_{12} in Ultrahigh Magnetic Fields. *J. Phys. Soc. Jpn.* **86**, 054710 (2017). doi:10.7566/JPSJ.86.054710
18. J. Yamaguchi, A. Sekiyama, S. Imada, H. Fujiwara, M. Yano, T. Miyamachi, G. Funabashi, M. Obara, A. Higashiya, K. Tamasaku, M. Yabashi, T. Ishikawa, F. Iga, T. Takabatake, S. Suga, Kondo lattice effects and the collapse of lattice coherence in Yb 1 – x Lu x B 12 studied by hard x-ray photoelectron spectroscopy. *Phys. Rev. B* **79**, 125121 (2009). doi:10.1103/PhysRevB.79.125121

19. Y. Utsumi, D. Kasinathan, K.-T. Ko, S. Agrestini, M. W. Haverkort, S. Wirth, Y.-H. Wu, K.-D. Tsuei, D.-J. Kim, Z. Fisk, A. Tanaka, P. Thalmeier, L. H. Tjeng, Bulk and surface electronic properties of SmB 6 : A hard x-ray photoelectron spectroscopy study. *Phys. Rev. B* **96**, 155130 (2017). doi:10.1103/PhysRevB.96.155130
20. H. Weng, J. Zhao, Z. Wang, Z. Fang, X. Dai, Topological crystalline Kondo insulator in mixed valence ytterbium borides. *Phys. Rev. Lett.* **112**, 016403 (2014). doi:10.1103/PhysRevLett.112.016403 Medline
21. Materials, methods and additional data are available as supplementary materials on Science Online.
22. J. C. Cooley, M. C. Aronson, Z. Fisk, P. C. Canfield, SmB6: Kondo insulator or exotic metal? *Phys. Rev. Lett.* **74**, 1629–1632 (1995). doi:10.1103/PhysRevLett.74.1629 Medline
23. F. Iga, N. Shimizu, T. Takabatake, Single crystal growth and physical properties of Kondo insulator YbB12. *J. Magn. Magn. Mater.* **177-181**, 337–338 (1998). doi:10.1016/S0304-8853(97)00493-9
24. K. S. D. Beach, P. A. Lee, P. Monthoux, Field-induced antiferromagnetism in the Kondo insulator. *Phys. Rev. Lett.* **92**, 026401 (2004). doi:10.1103/PhysRevLett.92.026401 Medline
25. K. Sugiyama, F. Iga, M. Kasaya, T. Kasuya, M. Date, Field-Induced Metallic State in YbB $_{12}$ under High Magnetic Field. *J. Phys. Soc. Jpn.* **57**, 3946–3953 (1988). doi:10.1143/JPSJ.57.3946
26. T. Takabatake, M. Nagasawa, H. Fujii, G. Kido, M. Nohara, S. Nishigori, T. Suzuki, T. Fujita, R. Helfrich, U. Ahlheim, K. Fraas, C. Geibel, F. Steglich, Anisotropic suppression of the energy gap in CeNiSn by high magnetic fields. *Phys. Rev. B Condens. Matter* **45**, 5740–5743 (1992). doi:10.1103/PhysRevB.45.5740 Medline
27. G. S. Boebinger, A. Passner, P. C. Canfield, Z. Fisk, Studies of the Kondo insulator Ce3Bi4Pt3 in 61 T pulsed magnetic fields. *Physica B* **211**, 227–229 (1995). doi:10.1016/0921-4526(94)00992-5
28. J. C. Cooley, M. C. Aronson, A. Lacerda, Z. Fisk, P. C. Canfield, R. P. Guertin, High magnetic fields and the correlation gap in SmB6. *Phys. Rev. B Condens. Matter* **52**, 7322–7327 (1995). doi:10.1103/PhysRevB.52.7322 Medline
29. J. C. Cooley, C. H. Mielke, W. L. Hults, J. D. Goettee, M. M. Honold, R. M. Modler, A. Lacerda, D. G. Rickel, J. L. Smith, *J. Supercond.* **12**, 171–173 (1999). doi:10.1023/A:1007771030747
30. S. Wolgast, Y. S. Eo, T. Öztürk, G. Li, Z. Xiang, C. Tinsman, T. Asaba, B. Lawson, F. Yu, J. W. Allen, K. Sun, L. Li, Ç. Kurdak, D.-J. Kim, Z. Fisk, Magnetotransport measurements of the surface states of samarium hexaboride using Corbino structures. *Phys. Rev. B* **92**, 115110 (2015). doi:10.1103/PhysRevB.92.115110
31. D. Shoenberg, *Magnetic Oscillations in Metals*, (Cambridge Univ. Press, Cambridge, 2009).
32. K. Hagiwara, Y. Ohtsubo, M. Matsunami, S. Ideta, K. Tanaka, H. Miyazaki, J. E. Rault, P. L. Fèvre, F. Bertran, A. Taleb-Ibrahimi, R. Yukawa, M. Kobayashi, K. Horiba, H. Kumigashira, K. Sumida, T. Okuda, F. Iga, S. Kimura, Surface Kondo effect and non-trivial metallic state of the Kondo insulator YbB12. *Nat. Commun.* **7**, 12690 (2016). doi:10.1038/ncomms12690 Medline
33. T. Terashima, PhD thesis, University of Tokyo.
34. M. Gurvitch, Ioffe-Regel criterion and resistivity of metals. *Phys. Rev. B* **24**, 7404–7407 (1981). doi:10.1103/PhysRevB.24.7404
35. L. Zhang, X.-Y. Song, F. Wang, Quantum Oscillation in Narrow-Gap Topological Insulators. *Phys. Rev. Lett.* **116**, 046404 (2016). doi:10.1103/PhysRevLett.116.046404 Medline
36. H. K. Pal, F. Piéchon, J.-N. Fuchs, M. Goerbig, G. Montambaux, Chemical potential asymmetry and quantum oscillations in insulators. *Phys. Rev. B* **94**, 125140 (2016). doi:10.1103/PhysRevB.94.125140
37. M. M. Altarawneh, C. H. Mielke, J. S. Brooks, Proximity detector circuits: An alternative to tunnel diode oscillators for contactless measurements in pulsed magnetic field environments. *Rev. Sci. Instrum.* **80**, 066104 (2009). doi:10.1063/1.3152219 Medline
38. S. Ghannadzadeh, M. Coak, I. Franke, P. A. Goddard, J. Singleton, J. L. Manson, Measurement of magnetic susceptibility in pulsed magnetic fields using a proximity detector oscillator. *Rev. Sci. Instrum.* **82**, 113902 (2011). doi:10.1063/1.3653395 Medline
39. J. Singleton, C. de la Cruz, R. D. McDonald, S. Li, M. Altarawneh, P. Goddard, I. Franke, D. Rickel, C. H. Mielke, X. Yao, P. Dai, Magnetic quantum oscillations in YBa2Cu3O6.61 and YBa2Cu3O6.69 in fields of up to 85 T: Patching the hole in the roof of the superconducting dome. *Phys. Rev. Lett.* **104**, 086403 (2010). doi:10.1103/PhysRevLett.104.086403 Medline
40. Y. Matsumoto, T. Terashima, S. Uji, N. Kimura, H. Aoki, How Are Heavy and Itinerant Electrons Born in a Dilute Kondo Alloy? *J. Phys. Soc. Jpn.* **81**, 054703 (2012). doi:10.1143/JPSJ.81.054703
41. T. Saso, M. Itoh, Insulator-to-metal transition in Kondo insulators under a strong magnetic field. *Phys. Rev. B Condens. Matter* **53**, 6877–6880 (1996). doi:10.1103/PhysRevB.53.6877 Medline
42. M. Jaime, R. Movshovich, G. R. Stewart, W. P. Beyermann, M. G. Berisso, M. F. Hundley, P. C. Canfield, J. L. Sarrao, Closing the spin gap in the Kondo insulator Ce3Bi4Pt3 at high magnetic fields. *Nature* **405**, 160–163 (2000). doi:10.1038/35012027 Medline
43. F. Iga, K. Suga, K. Takeda, S. Michimura, K. Murakami, T. Takabatake, K. Kindo, Anisotropic magnetoresistance and collapse of the energy gap in Yb $_{1-x}$ Lu $_x$ B $_{12}$. *J. Phys. Conf. Ser.* **200**, 012064 (2010). doi:10.1088/1742-6596/200/1/012064
44. I. Milat, F. Assaad, M. Sigrist, Field induced magnetic ordering transition in Kondo insulators. *Eur. Phys. J. B* **38**, 571–580 (2004). doi:10.1140/epjb/e2004-00154-5
45. T. Ohashi, A. Koga, S. Suga, N. Kawakami, Field-induced phase transitions in a Kondo insulator. *Phys. Rev. B* **70**, 245104 (2004). doi:10.1103/PhysRevB.70.245104
46. M. A. Avila, S. L. Bud'ko, C. Petrovic, R. A. Ribeiro, P. C. Canfield, A. V. Tsvyashchenko, L. N. Fomicheva, Synthesis and properties of YbB2. *J. Alloys Compd.* **358**, 56–64 (2003). doi:10.1016/S0925-8388(03)00051-3
47. J. Y. Kim, B. K. Cho, H. J. Lee, H.-C. Kim, Low dimensional intermediate valence fluctuation in single crystalline YbB4. *J. Appl. Phys.* **101**, 09D501 (2007). doi:10.1063/1.2667727
48. D. J. Kim, J. Xia, Z. Fisk, Topological surface state in the Kondo insulator samarium hexaboride. *Nat. Mater.* **13**, 466–470 (2014). doi:10.1038/nmat3913 Medline
49. D. Shoenberg, The de haas-van alphen effect in copper, silver and gold. *Philos. Mag.* **5**, 105–110 (1960). doi:10.1080/14786436008243292
50. H. K. Pal, Quantum oscillations from inside the Fermi sea. *Phys. Rev. B* **95**, 085111 (2017). doi:10.1103/PhysRevB.95.085111

ACKNOWLEDGMENTS

We thank R. Peters, H. Shishido, Kai Sun, T. Senthil, Patrick Lee, and Y. Tokiwa for valuable discussions. **Funding:** This work is mainly supported by he National Science Foundation under Award No. DMR-1707620 (high field magnetization and resistivity measurements), by the Office of Naval Research through the Young Investigator Prize under Award No. N00014-15-1-2382 (sample structure and low field electrical transport characterizations), by Grants-in-Aid for Scientific Research (KAKENHI) (Nos. 25220710, 15H02106, 15H03688, 16K05460, 16K13837) and on Innovative Areas Topological Material Science (No. 15H05852) from Japan Society for the Promotion of Science (JSPS). The synchrotron radiation X-ray powder diffraction measurements were carried out at BL02B2/SPring-8 in Japan (Proposal No. 2017A1856). Some results are obtained with equipment supported by he National Science Foundation Major Research Instrumentation award under No. DMR-1428226 (the equipment of the thermodynamic and electrical transport characterizations). The development of the torque magnetometry technique in intense magnetic fields was supported by the Department of Energy under Award No. DE-SC0008110. A portion of this work was performed at the National High Magnetic Field Laboratory, which is supported by National Science Foundation Cooperative Agreement No. DMR-1644779 and DMR-1157490, the Department of Energy (DOE) and the State of Florida. J.S. acknowledges support from the DOE BES Program "Science in 100 T". The experiment in NHMFL is funded in part by a QuantEmX grant from ICAM and the Gordon and Betty Moore Foundation through Grant GBMF5305 to Z, X., T. A., L. C., C. T., and L. L.. We are grateful for the assistance of Tim Murphy, Hongwoo Baek, Glover Jones, and Ju-Hyun Park of NHMFL. T.A. thanks the Nakajima Foundation for support. B.J.L. acknowledges support by the National Science Foundation Graduate Research Fellowship under Grant No. F031543 and the National Science Foundation East Asia and Pacific Summer Institute Fellowship award No. 1614138. **Author contibutions:** L.L. and T.M. designed the expeirments. Z.X. preformed the experiments on the quantum oscillation measurements and analyzed the data on YbB_{12} with the assitance by T.A., B.L., C.T., L.C. J.S. and L.L.. G.L. performed the supporting oscillation measurements

in YbB_6. Y.K. preformed the supporting Xray studies and SdH simulations with the aisstance by K.S., H.K, Y.S. and Y.M.. S.Y. Y.L.C. and F.I. provided the samples. Z.X. Y.K. Y.M. and L.L. wrote the manuscript with the assitance from all the authors. **Competing interests:** Authors declare no competing interests. **Data and materials availability:** All the data in the manuscript main text are avaialble as csv ASCII files in the supplmental materials.

SUPPLEMENTARY MATERIALS

www.sciencemag.org/cgi/content/full/science.aap9607/DC1
Materials and Methods
Supplementary Text
Figs. S1 to S13
Table S1
References (*37–50*)
Data File S1

14 September 2017; accepted 20 August 2018
Published online 30 August 2018
10.1126/science.aap9607

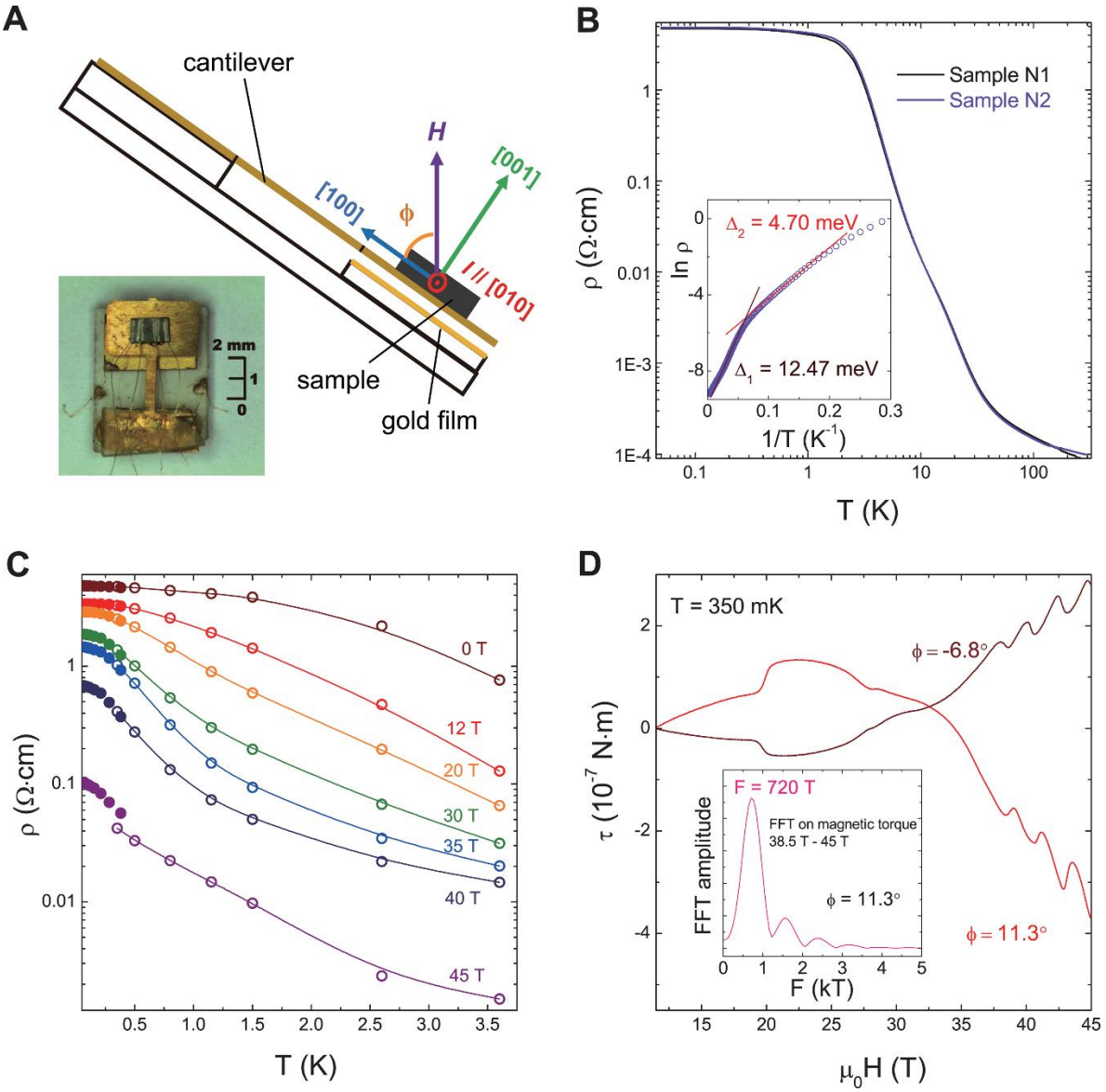

Fig. 1. Electrical transport and magnetic torque measurements in YbB_{12}. (A) Sketch of the experimental setup [for details see (*21*)] and the definition of tilt angle ϕ with respect to the magnetic field. Inset: Photograph of a YbB_{12} single crystal (sample N2) mounted onto a cantilever beam magnetometer, with four gold wires attached to the crystallographic (001) surface for the transport measurement. (B) Resistivity of two YbB_{12} single crystals plotted as a function of temperature. The inset shows the Arrhenius plot, $\ln\rho$ vs. $1/T$. According to the thermal activation model, the slope of the Arrhenius plot equals $\Delta/2k_B$, with Δ the bandgap width and k_B the Boltzmann constant. Linear fitting in two different temperature ranges, 20 K < T < 40 K and 6 K < T < 2.5 K, yields two characteristic gap widths, 12.5 meV and 4.7 meV, respectively. (C) Resistivity of YbB_{12} sample N2 under different magnetic fields from 0 T to 45 T, plotted against temperature. Hollow and solid symbols are data taken in ^{3}He cryostat at $\phi = 7.4°$ and in dilution fridge at $\phi = 8.5°$, respectively. Solid lines are guides to the eye. (D) Magnetic torque in YbB_{12} measured at T = 350 mK and at two different tile angles, $\phi = -6.8°$ and $\phi = 11.3°$. Both exhibit strong quantum oscillations under high magnetic fields. The amplitude of the oscillatory part of magnetic torque at $\phi = 11.3°$ is ~6 × 10^{-8} N · m at the highest field, corresponding to an effective transverse magnetization of ~1.4 × 10^{-9} A· m^2 (1.51 × 10^{14} μ_B). Inset: FFT on the magnetic torque signal with $\phi = 11.3°$ reveals a major peak at F = 720 T and its harmonics.

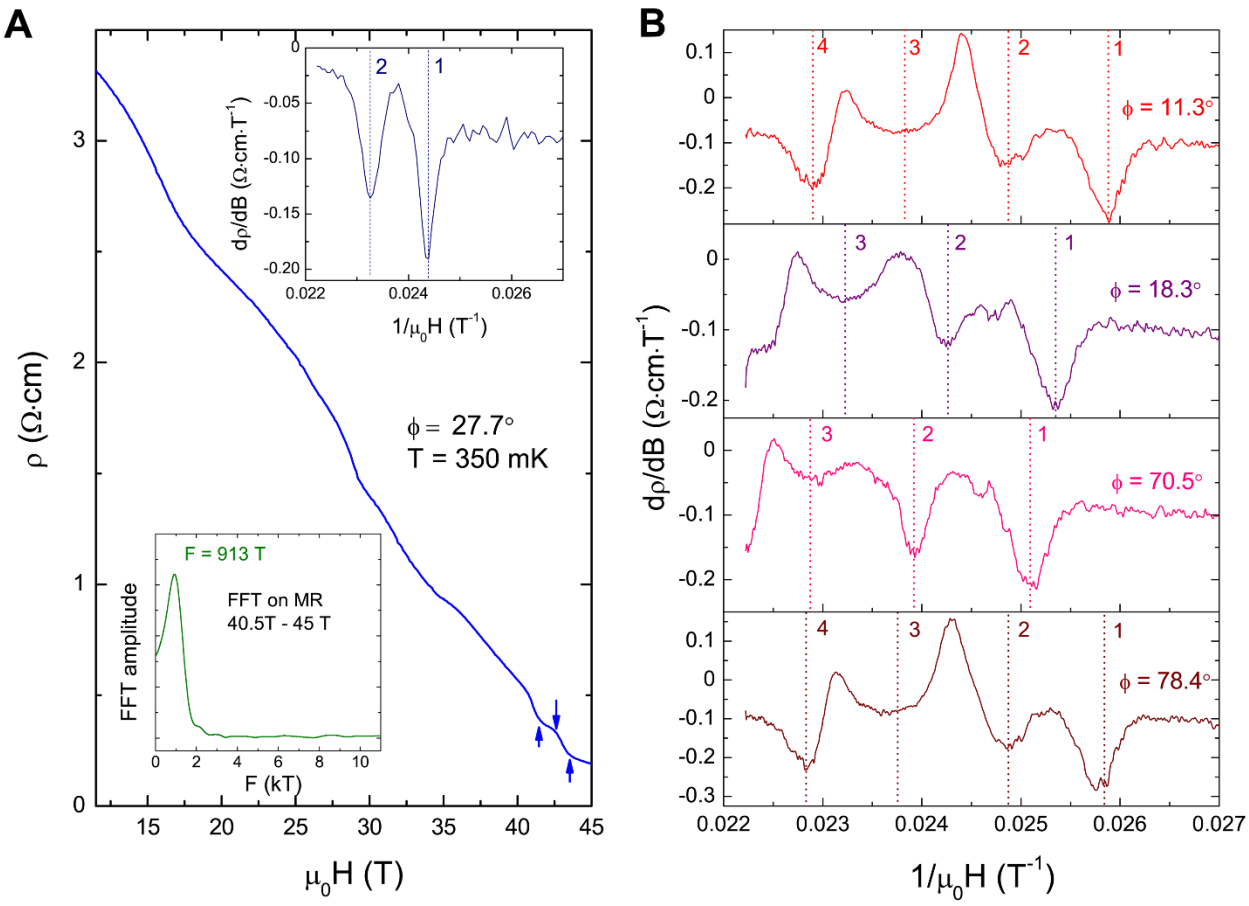

Fig. 2. Resistivity and electrical oscillations in intense magnetic fields in YbB_{12}. (A) Resistivity of sample N2 as a function of magnetic field measured up to 45 T taken at $T = 350$ mK at a tilt angle $\phi = 27.7°$. Quantum oscillations are clearly observed at high magnetic field beyond 40.8 T. The extrema are marked by arrows. Upper inset: first magnetic field derivative of resistance has two prominent valleys and one peak. Lower inset: FFT on the magnetoresistance data presented between $\mu_0 H = 40.5$ T and 45 T. A single peak frequency of $F = 913$ T is resolved. (B) Field derivative of sample resistivity at four different tilt angles. Dotted lines mark the approximately evenly spaced valleys of SdH oscillation. Three to four periods in total can be observed, depending on the field orientation. The oscillation pattern at ϕ is repeated at $90° - \phi$, consistent with the cubic symmetry of crystal structure.

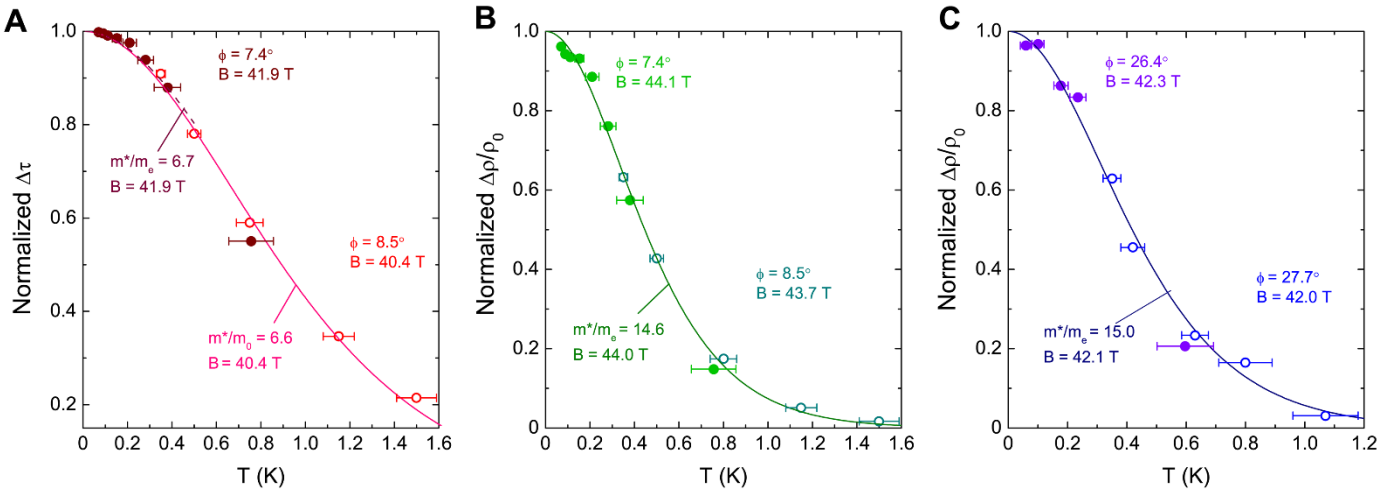

Fig. 3. Effective mass fitting on dHvA and SdH oscillations in YbB_{12}. (A) Normalized dHvA oscillation amplitude $\Delta\tau$ as a function of temperature. Hollow circles and solid circles are the data taken in ^{3}He cryostat at $\phi = 8.5°$ and in portable dilution fridge at $\phi = 7.4°$, respectively. The LK model fitting using parameters $m^* = 6.6\ m_e$, $B = 40.4$ T is presented by solid line based on the ^{3}He cryostat data. In comparison, the LK fitting based on the portable dilution fridge data gives $m^* = 6.7\ m_e$, $B = 41.9$ T, presented in the dashed line. (B and C) Temperature dependence of normalized SdH amplitude $\Delta\rho/\rho_0$. (B) is taken at the same tilt angle as in (A), and (C) is taken at a tilt angle close to that in Fig. 2A. Hollow and solid symbols are data measured in portable ^{3}He cryostat and dilution fridge, respectively. Here ρ_0 is the zero-field resistivity at corresponding temperatures. Solid lines are fittings based on the LK formula, with parameters shown in each panel. According to the fittings, SdH effective mass exhibits a weak anisotropy between $\phi \simeq 8°$ [(B), $m^* = 14.6\ m_e$) and $\phi \simeq 27°$ ((C), $m^* = 15.0\ m_e$]. In all three panels, the quantum oscillation amplitudes (raw data shown in fig. S5) are taken as the averaged value of an adjacent peak and valley obtained after subtracting a polynomial background from the raw data, and the effective magnetic field for each data sets is an inverse average of the peak and valley positions. [Details of the background subtraction and the determination of the B parameters in the LK fittings are presented in Section 6 of (*21*)]. The error bars on the temperature are estimated based on the magnetoresistance effect on the ruthenium oxide thermometer above 11.4 T.

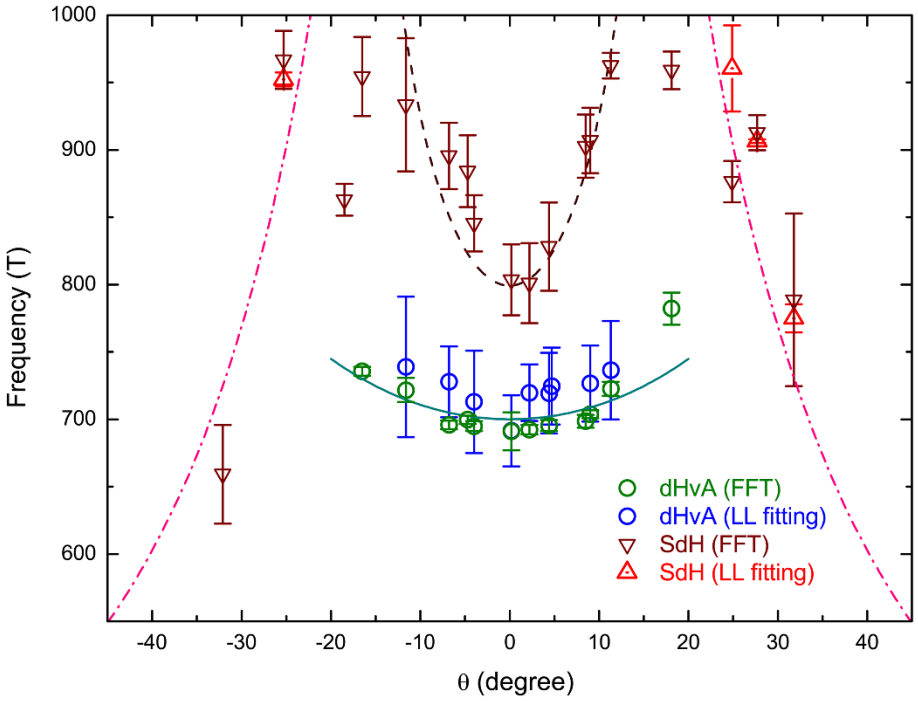

Fig. 4. Angular dependence of quantum oscillation frequencies. The frequencies of the quantum oscillations appearing at high field in YbB_{12}. Magnetic field H is rotated in a plane perpendicular to the current direction, and the effective tilt angle θ is defined as the angle between H and the equivalent crystal axes [001]/[100] in a cubic structure. Circles are dHvA frequencies obtained from FFT (green) and the slope of a linear fitting of the LL index versus inverse magnetic field (blue). The solid line is a calculation using two-dimensional (2D) Fermi surface model: $F = F_0/\cos\theta$ with $F_0 =$ 700 T. Up triangles (red) and down triangles (brown) are SdH frequencies acquired from the FFT and from the linear fitting of the LL index plot, respectively. The dashed line is the fitting by a hyperboloid model representing a Fermi surface neck region with the principle axis along the [001] direction, whereas the dash-dot lines are simulation for the high-angle data points using an oblate spheroid model with the principle axis along [001] direction. For the detailed parameters in these models, see Section 8 of (*21*). The error bars come from the difference between different sampling windows for the FFT results, and from the linear fitting error for the LL analysis.

Quantum oscillations of electrical resistivity in an insulator

Z. Xiang, Y. Kasahara, T. Asaba, B. Lawson, C. Tinsman, Lu Chen, K. Sugimoto, S. Kawaguchi, Y. Sato, G. Li, S. Yao, Y. L. Chen, F. Iga, John Singleton, Y. Matsuda and Lu Li

published online August 30, 2018